

RESEARCH ARTICLE

The morphology and characterization of nanostructured α -PbO prepared from spent lead acid battery negative plate

Samiha Redaoui*, Achour Dakhouché

Laboratory of inorganic materials, Departement of chemistry, Faculty of science, University of M'sila, University pole, Road Bourdj Bou Arreiridj, Msila 28000-Algeria

*Corresponding author: Samiha Redaoui, samiha.redaoui@univ-msila.dz

ABSTRACT

The increase in global energy consumption is paralleled by an increase in the waste generated from it, especially those related to used batteries which constitute a source of contamination of the environment and a great threat for the human health. Therefore, it has become more necessary to work on recycling batteries to revalue their active materials and to preserve the environment. The aim of this work was the synthesis and characterization of nanostructured PbO obtained from spent lead acid batteries negative plate. The negative plates of used battery are made up of large amounts of PbSO₄ and smaller amounts of Pb. The PbSO₄ was desulfated with (NH₄)₂CO₃ to obtain PbCO₃ which is then calcined in air at different temperatures. In this work we are interested in studying the effect of temperature on the nature and the morphology of the products of the calcination process. The results show that at a 450°C we obtain α -PbO, at 500°C β -PbO, after these temperatures we get a mixture of lead oxides α -PbO, β -PbO, and minium Pb₃O₄. α -PbO granules have sizes around 26 nm with a mesoporous materials and BET surface area was equal to about 4 m²/g.

Keywords: lead; nanostructured PbO; Lead acid battery; lead oxides, waste recycling

ARTICLE INFO

Received: 11 March 2025
Accepted: 26 April 2025
Available online: 28 May 2025

COPYRIGHT

Copyright © 2025 by author(s).
Applied Chemical Engineering is published by Arts and Science Press Pte. Ltd. This work is licensed under the Creative Commons Attribution-NonCommercial 4.0 International License (CC BY 4.0).
<https://creativecommons.org/licenses/by/4.0/>

1. Introduction

Batteries are ubiquitous in our world today, powering everything from our phone, calculators, cars, they are essential, the lead accumulator was the first rechargeable battery invented in 1859 by the French physicist Gaston Planté, Today it represents the storage system of electricity most used in industry and in vehicle equipment.^[1,2] His report energy/weight is modest (35Wh/kg) but its ability to provide high intensities of current places its power/weight ratio at an honorable level. These united characteristics with its low cost, and mature technology, keep the lead acid battery attractive for many applications.^[3,4] But we also need to think about what happens when they are no longer useful. Throwing them away isn't the best idea, recycling is the ideal way to make use of waste^[5]. The objective of recycling processes is to separate the constituents into different fractions which can be reintroduced into a production process, by treating the dangerous fractions and by minimizing process waste (effluents, emissions), energy consumption and costs^[6]. So far, many routes, either pyrometallurgical or hydrometallurgical, have been employed to produce metallic lead from the spent lead acid batteries. However, pyrometallurgical routes require high temperature (around 1000 °C), which not only consume huge amounts of energy but also easily produce SO₂ and lead dust if the desulfation is not fully completed, bringing secondary contamination to the environment^[7,8]

The $(\text{NH}_4)_2\text{CO}_3$ desulfurization- calcination route is more energy efficient : unlike high-temperature pyrometallurgical routes, this method operates at lower temperature ,reducing energy, consumption and improving process efficiency, more cost-effective : the use of ammonium carbonate a low-cost, readily available chemical, and more selected capturing sulfur compounds, offering superior desuffurisation with minimal side reaction ,contrasts with the more expensive reagent or complex processes involved in pyrometallurgy, more environmentally friendly: the process produce fewer byproducts and minimizes emissions, contributing to cleaner, more sustainable operations compared to the often pollutive nature of pyrometallurgical methods.

This paper highlights the importance of recycling batteries to be able to prepare important materials economically and to protect the environment and humans from toxic battery waste. Lead oxide nanostructure is one of the metal oxides that have important applications in storage batteries, the glass industry, and pigments. Many processes have been used to synthesize PbO nanostructures, such as thermal decomposition^[9], anodic oxidation^[10], a sonochemical method^[11], a hydrothermal method^[12], and calcination^[13]. In this paper we worked on re-evaluating the active materials present in the negative plates of a used battery by preparing nano-lead oxide. The processes of synthesis comprise: Prepare samples by separating the positive plates from the negative plates of the used battery, manually removing the paste (active material),washing it well with distilled water to get rid of sulfuric acid and suspended materials, then drying it. Desulfation with amonium carbonate $(\text{NH}_4)_2\text{CO}_3$, Calcination at different temperatures to eliminate carbonates in the form of carbon dioxide gas CO_2 and obtain lead oxides. At each stage of the above process, the chemical composition and the morphology of the obtained materials was studied by X-Ray diffraction, scanning electronic microscopy SEM, IR and measuring surface area BET.

2. Materials and methods

2.1. Materials

Ammonium carbonate $(\text{NH}_4)_2\text{CO}_3$ (98%) were purchased from Sigma-Aldrich (Australia). All aqueous solutions were prepared with deionized water, clacining furnace from Carbolite (England, max temperature 1200°C , at a steady rate of 20°C per minute in static air), The initial active mass was procured from end-of-lif Starting, Light, and Ignition (SLI) lead acid battery (ENPEC 60 AH,12v made in setif, Algeria).

2.2. Methods

2.2.1. The experimental method for preparing lead oxide from a used battery:

To prepare lead oxide from the negative plate of a used battery, we followed the following experimental method. Manually removing the paste of negative plate of used battery, washing it well with distilled water (24 h) to get rid of sulfuric acid and suspended materials, then drying it at 80°C for 24 h. The desulfation of PbSO_4 was carried out as follows: 10 g of negative active masse was added to 50 mL of 0.8 mol. L^{-1} $(\text{NH}_4)_2\text{CO}_3$ solution. The suspension was vigorously stirred at 30°C for 120 min. The resultant was filtered and washed three times with water and then dried at 100°C for 12 h. The sample was then calcined at 400, 450,500,550 and 600°C , respectively, for 1 hour in air to find out the best temperature for preparation of $\alpha\text{-PbO}$.

2.2.1. X-ray diffraction analysis XRD

Using an XRD Porto bench top (Canada) powder diffraction system and monochromatic $\text{Cu-K}\alpha$ radiation, powder X-ray diffraction (XRD) patterns were captured. They were captured throughout a $10\text{--}80$ degree angular range with 0.02 degree increments and a 2s step-counting interval. $\text{K}\alpha$ radiation was obtained from a copper x-ray tube operating at 40kV and 30mA . Using the X'pert HighScore Plus software (Malvern Analytical, United Kingdom), the patterns were processed and analyzed. The Crystallography Open Database (COD, 2019) and the American Mineralogist crystal structure database were used to identify the phases.

The average crystalline size of the prepared PbO nanoparticles was calculated by applying the Debye-Scherrer equation^[14,15]

$$D = K\lambda / \beta \cos \theta \quad (1)$$

Where D is the crystalline size of the nanoparticles, K is Scherrer's constant (0.89), λ is the wavelength of X-ray (1.54 Å) used in XRD, β is the full width at maxima (FWHM) of the high-intensity diffraction peak and θ is the angle of Bragg's diffraction (by Origin Pro 8.5).

2.2.2. Infra-Red analysis

A Cary 660 spectrophotometer from Agilent Technologies, (Australia), was used to analyze the products of each stage of the process of synthesis of nanostructured PbO from used battery, KBr was utilized as a support, and the spectral range under investigation ranged from 4000cm⁻¹ to 400 cm⁻¹

2.2.3. Scanning electron microscopy analysis SEM

A field emission scanning electron microscope, Sigma 360 VP (ZEISS, Germany), from the Technical Platform for Physicochemical Analyzes (PTAPC OUARGLA) Algeria, was used to verify the morphology and the composition of nanostructured α -PbO .

2.2.4. Thermogravimetric analysis TGA

The specific surface area of nano structured α -PbO was determined by nitrogen adsorption at 77 K using an instrument (Micrometrics ASAP20, USA)

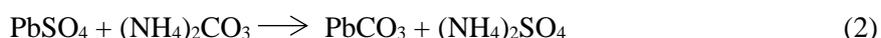
2.2.5. Brunauer-Emmett-Teller (BET) surface area analysis

Using a TGA-51 analyzer (Shimadzu, Japan) in the Laboratory of Inorganic Materials in M'sila University, the thermogravimetric studies were performed. In a flowing nitrogen environment (20cm³ per minute), samples were heated to 600°C at a steady rate of 10°C per minute.

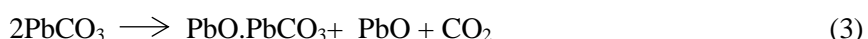
3. Results

3.1. X-ray diffraction

The materials resulting from each stage were studied by XRD (**Figure 1**) to determine their composition, It can be noted that the primary active material (NAM 0) is a mixture of Pb and PbSO₄^[20,21] we can observe many phases. In the first stage, after desulfation, (NAM 1), we notice the disappearance of the peaks characteristic of PbSO₄ and the appearance of the peaks characteristic of PbCO₃^[19,22] according to the reaction (2)



As for the calcination stage, the oxidation of PbCO₃ to produce PbO and CO₂ takes place in stages, as shown in the reaction (3), (4) and (5), it can be observed: incomplete decomposition at 400°C of PbCO₃. the product consists of two phases PbCO₃-PbO and PbO. At 450°C the PbCO₃-PbO phase disappears, single phase α -PbO is formed. With the further increase of the temperature to 500 °C, β -PbO phase appears. α -PbO transfers into β -PbO if calcination temperature is 500 °C because it is well known that the transition takes place at about 488 °C^[18]. Therefore, 450 °C is the best temperature for preparation of α -PbO.



When PbCO₃ is calcined at 550°C, 600°C. α PbO is formed again with small presence of β PbO. we noted too the appears of minium Pb₃O₄ at this temperatures according the reaction, It is known that PbO can be oxidized in air, and it can certainly be accelerated at higher temperatures^[23] as showing in reaction (6), It can be seen that the XRD patterns at 550, and 600°C are almost identical.

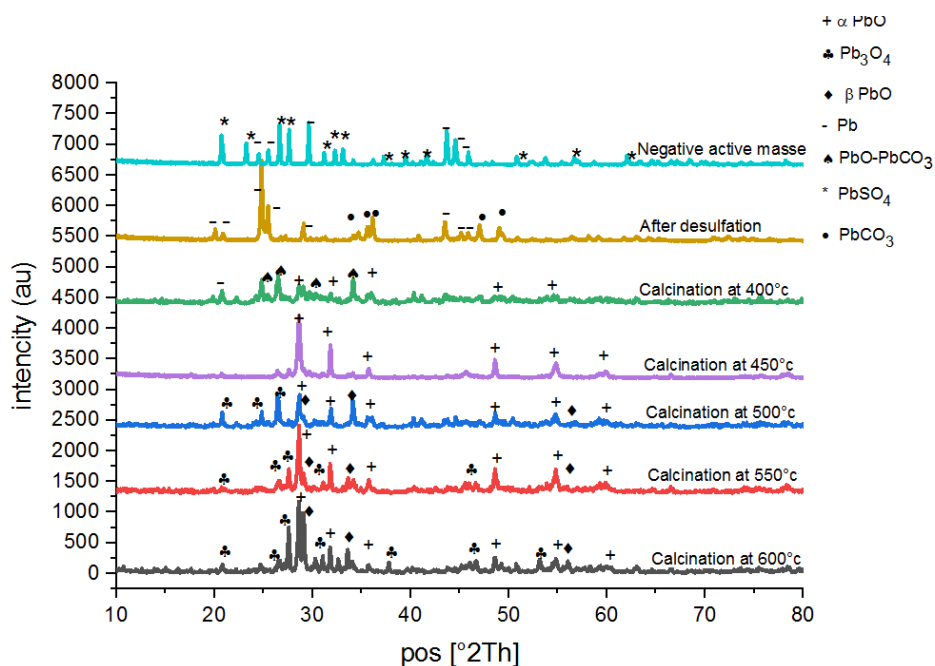
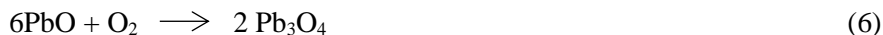


Figure 1. XRD pattern of products of each stage of process of synthesis of nanostructured PbO.

3.2. Size of grains

By applying the Debye- Scherer equation, we calculate the size of grains (Table.1). the results shows that we have obtained a nano structured lead oxides by the thermal method^[16,17] with a diameter ranging between 21-40nm

Table 1. Size of grains of lead oxide nanostructured.

Sample	Peak position	FWHM	D = Kλ / β cos θ
Calcination at 400°C	24,72	0,25	31,0406237
	25,29	0,23	33,7026145
	52,07	0,18	39,6563943
Calcination at 450°C	26,3174	0,29321	26,3827898
	28,58106	0,26671	28,8645542
	33,98822	0,26421	28,7551573
Calcination at 500°C	26,38	0,36	21,4853019
	34,1	0,34	22,3386222
	30,8	0,31	24,7066211
Calcination at 550°C	26,43	0,36	21,4831027
	30,85	0,32	23,9316603
	47,59	0,33	22,0272236
Calcination at 600°C	26,42	0,35	22,0973584
	28,68	0,33	23,3235432
	30,85	0,31	24,7036493

3.3. IR analysis

Fourier-transform infrared (FTIR) spectroscopy was employed to monitor the chemical evolution of the PbO material at different stages of the synthesis process. Each spectrum reveals key vibrational features that provide insight into the structural and compositional changes occurring throughout the multi-step conversion from spent battery paste to nanostructured PbO. The obtained FTIR spectra are shown in (Figure 2).

The infrared spectrum (Figure 2) shows absorptions in the following areas that are characteristic of: 1182cm^{-1} (S=O), 619cm^{-1} (S-O) we notice the presence of these two peaks in the primary active materials (NAM 0) and their complete disappearance in the rest of the stages after desulfation^[24]. 1725cm^{-1} (C=O), 820cm^{-1} (C-O) we notice the absence of these two peaks in the primary active materials (NAM 0)^[25], and then they appear in the second stage (NAM 1), where the transformation of PbSO_4 to PbCO_3 , in the stage of calcination at 400°C a quantity of carbonate remained, after this temperature ($450, 500, 550, 600^\circ\text{C}$) all carbonates are converted into CO_2 . A small peak located at about 458cm^{-1} , 680cm^{-1} , 470cm^{-1} , 694cm^{-1} corresponding to the (Pb-O-Pb), structural units was observed in the host matrix. Absorption bands located at about 1000 and 1100cm^{-1} are attributed to Pb-O asymmetric stretching vibrations in $[\text{PbO}_n]$ structural units^[26].

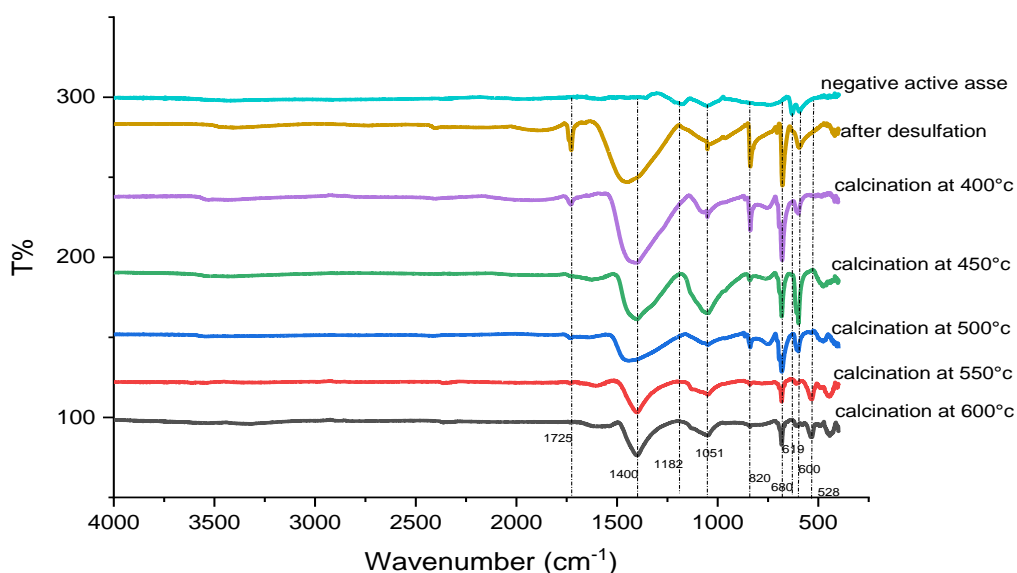
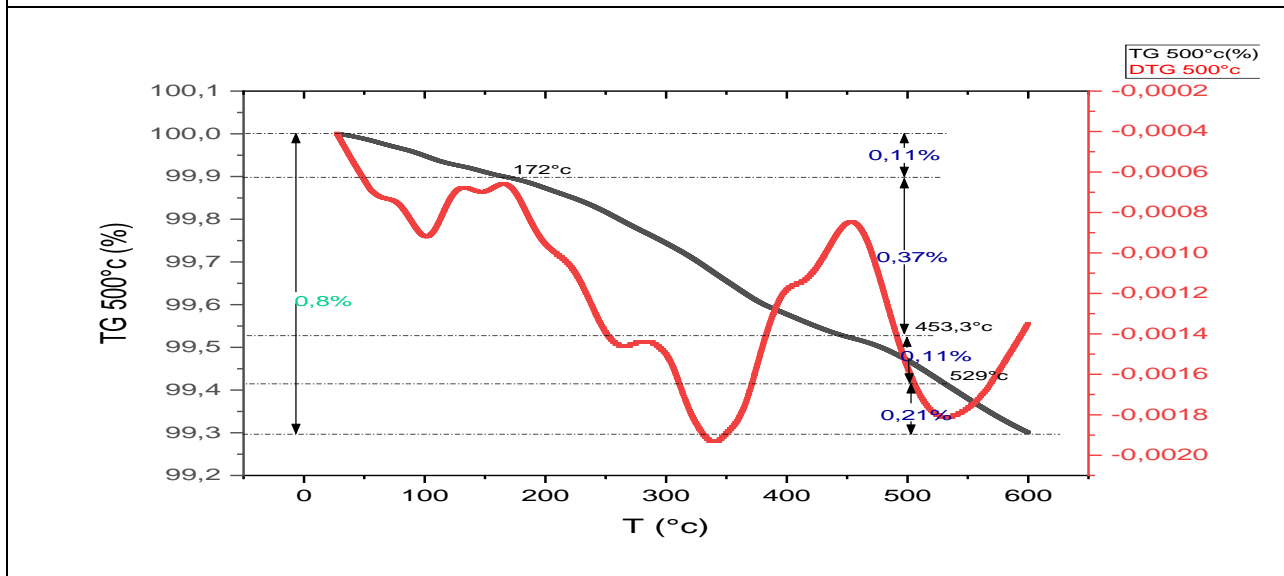
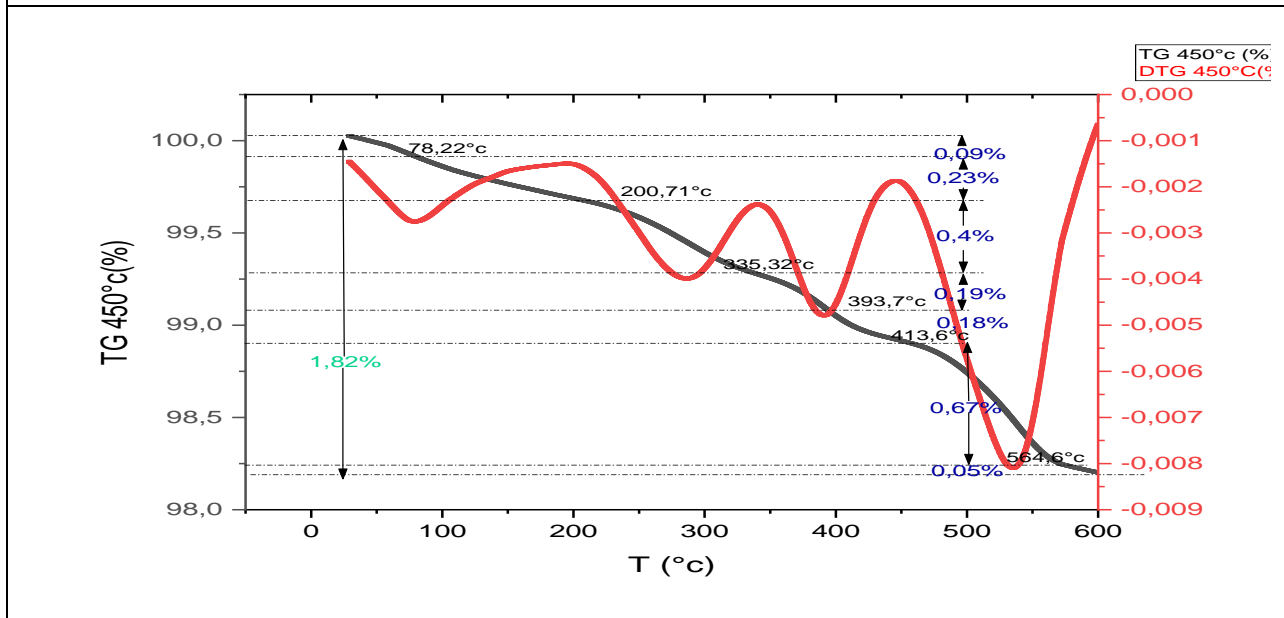
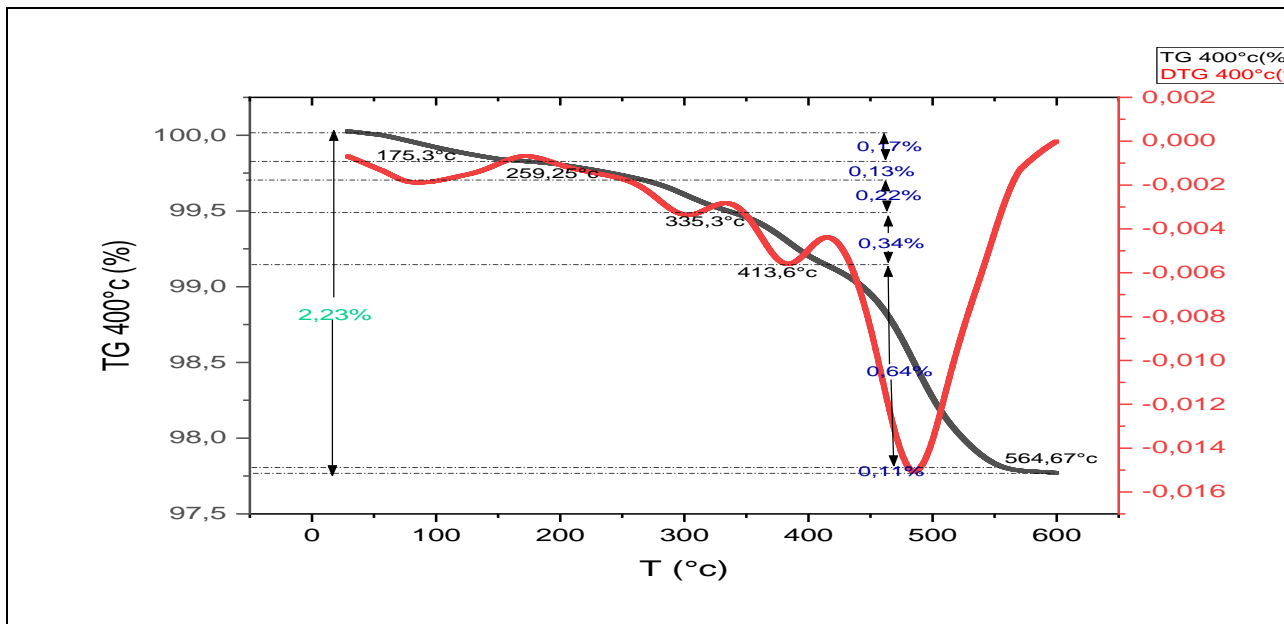


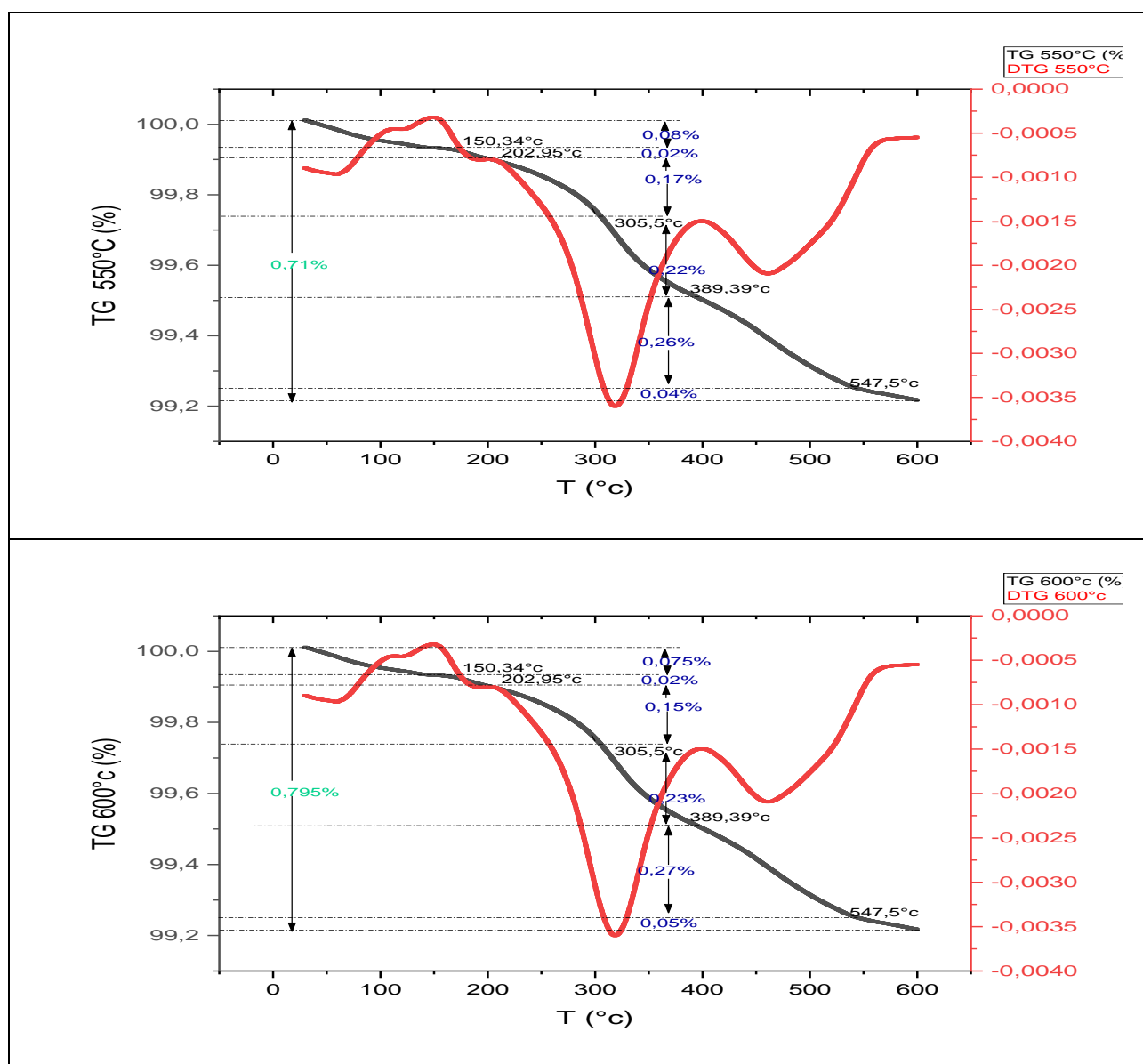
Figure 2. Infrared spectrum of the products of each stage of process of synthesis of nanostructured PbO.

3.4. TG analysis

Thermogravimetric analysis (TGA) is a powerful technique used to assess the thermal stability, compositional evolution, and decomposition behavior of materials as a function of temperature. In the present study, TGA was employed to monitor the thermal transformations of Pb-based precursors. The weight loss trends and the corresponding endothermic events observed in the derivative thermogravimetric (DTG) curves offer critical insights into the nature of the residual components, the removal of water and organics, the decomposition of sulfate or carbonate intermediates, and the overall thermal stability of the resulting PbO structures. The TGA and DTG thermograms are shown in (Table. 2).

Table. 2. TG and DTG thermograms at differents temperatures.





For the negative active masse sample calcined at 400°C, the thermal profile exhibited distinct behavior. A modest weight loss of 0.3% between 35–260 °C corresponds to the desorption of adsorbed water and possibly ammonia or loosely bound ammonium carbonate^[36]. Between 260 and 335 °C, a prominent endothermic peak in the DTG curve was associated with a 0.22% weight loss, attributed to the decomposition of intermediate lead carbonate species formed during the chemical reaction with ammonium carbonate^[37]. Subsequent endothermic decompositions were observed between 385–580 °C and 580–700 °C, accounting for 0.98% and 0.11% of mass loss, respectively. These stages may represent the stepwise breakdown of basic lead carbonates and partial transition to PbO^[38].

In contrast, the negative active masse sample calcined at 450, 500, 550, and 600°C, exhibited the highest thermal stability among all the samples. A negligible weight loss was recorded between 35– ~ 220 °C (max ~ 0.32%), corresponding to minor surface-bound water. The second stage, from 220– ~ 450 °C (max ~ 0.7%), showed a relatively low weight loss, possibly associated with the removal of residual organics or final traces of decomposition intermediates. The subsequent temperature ranges 450–600 °C and 600–700 °C involved only minor weight changes (max ~ 0.21%), indicating that nearly all volatile and labile components had been removed during the calcination step. The high residual mass confirms the formation of a stable, thermally robust PbO phase^[38].

3.5. SEM analysis

The particle size of nanostructured materials plays a crucial role in determining their physicochemical properties, including reactivity, surface energy, and functional performance in various applications. In the case of PbO derived from spent lead-acid battery negative plates, understanding particle size is essential for optimizing its use in catalysis, energy storage, and adsorption processes. The size of the particles directly affects the material's surface area, porosity, and overall efficiency in applications requiring high surface interactions. Therefore, accurate characterization of particle size using different analytical techniques is necessary to validate the obtained nanostructure and correlate the results with its performance.

The SEM micrographs and EDS for the samples of each stage of process of preparation of lead oxide are shown in Tables 3,4,5,6,7,8 and 9.

Table 3. SEM image of the initial negative active mass.

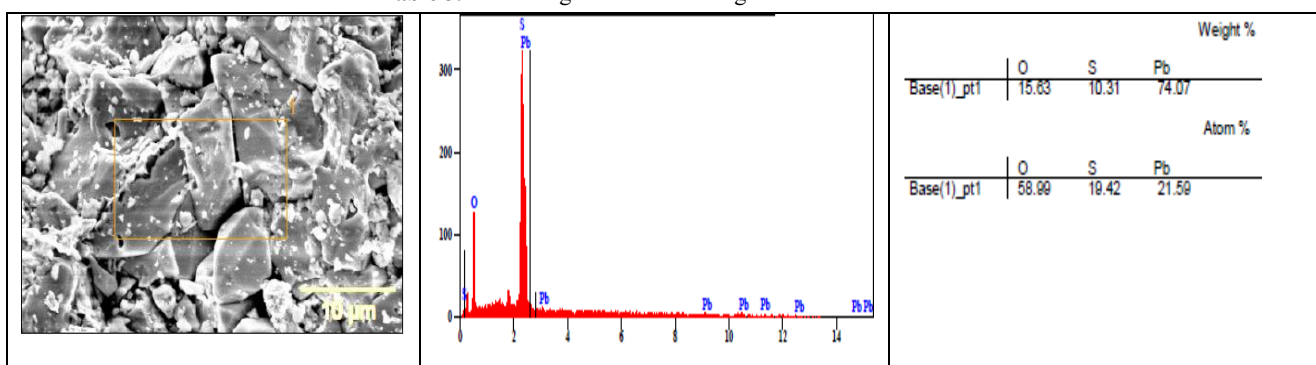


Table 4. SEM image of the negative active mass after desulfation.

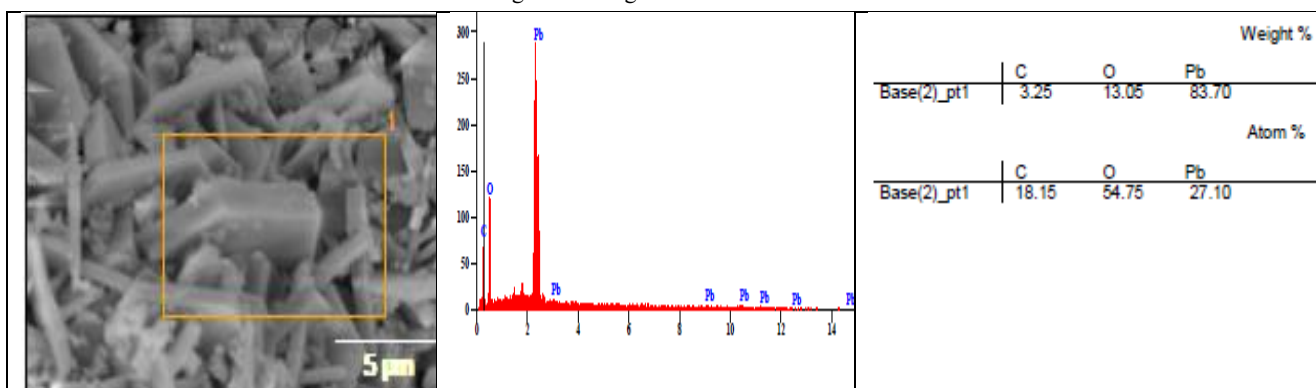


Table 5. SEM image of the negative active mass after calcination at 400°C.

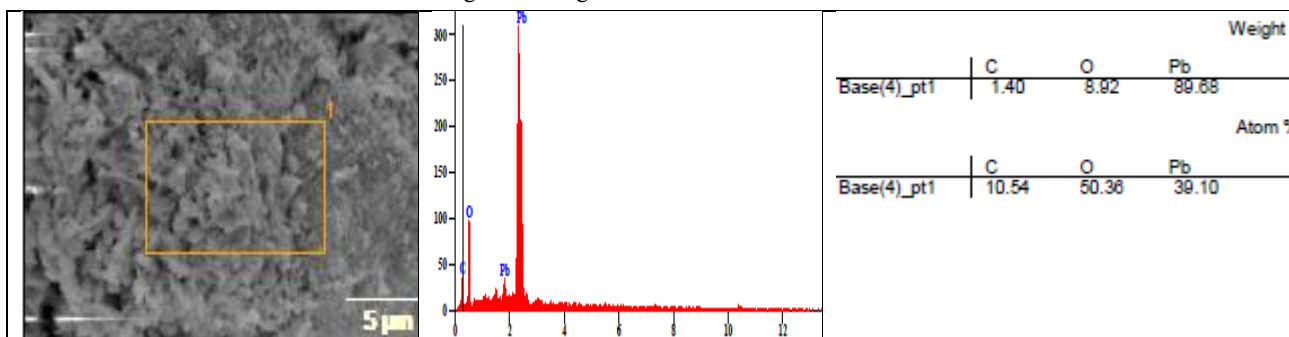


Table 6. SEM image of the negative active mass after calcination at 450°C.

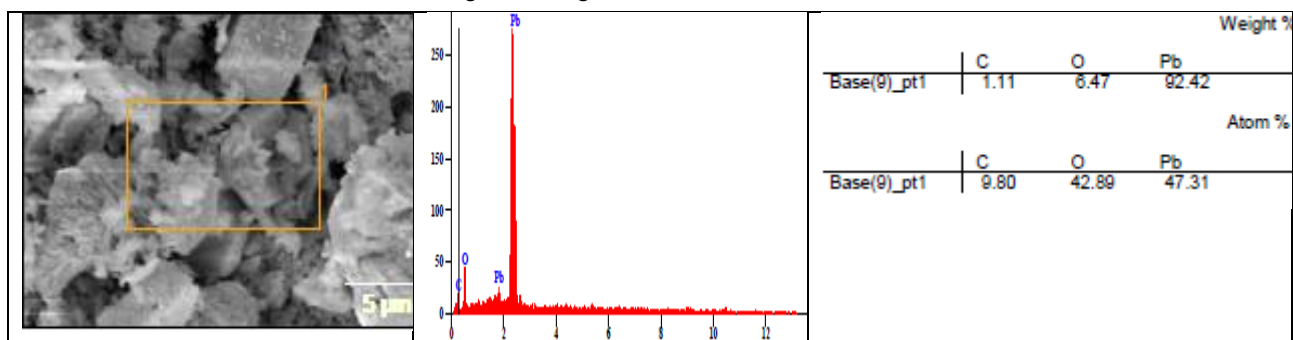


Table 7. SEM image of the negative active mass after calcination at 500°C.

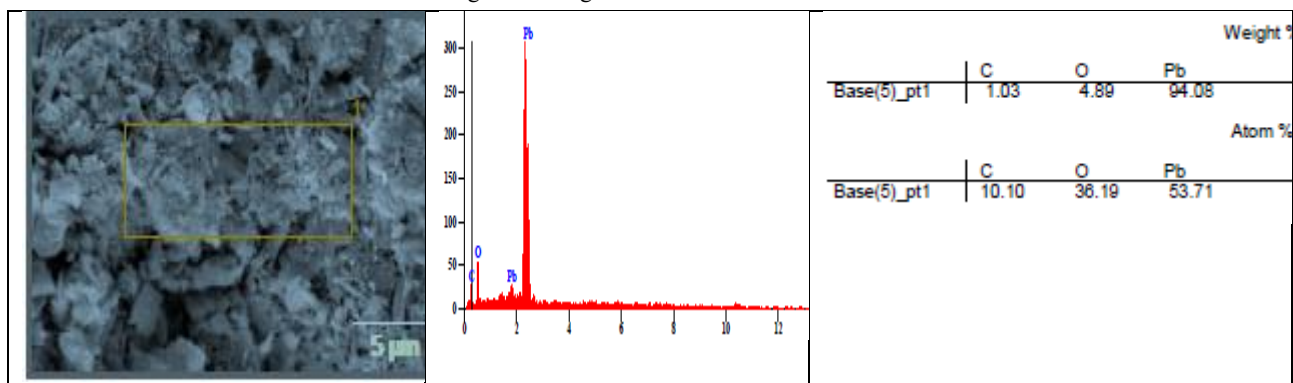


Table 8. SEM image of the negative active mass after calcination at 550°C.

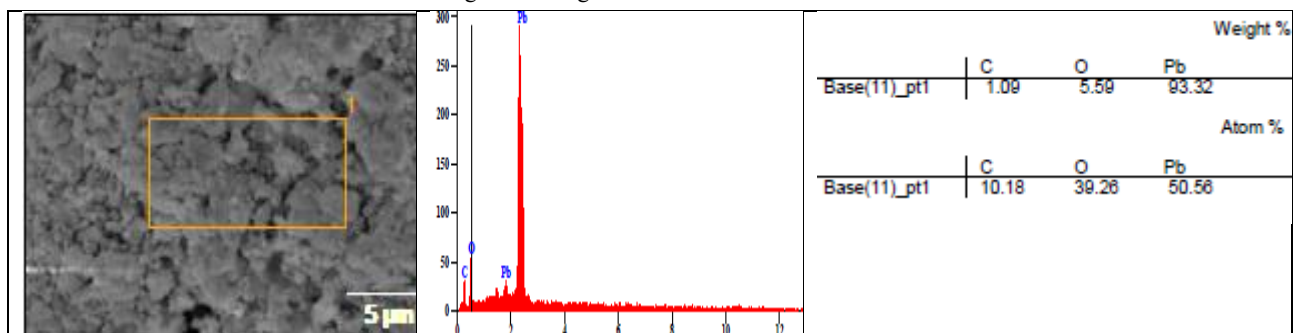
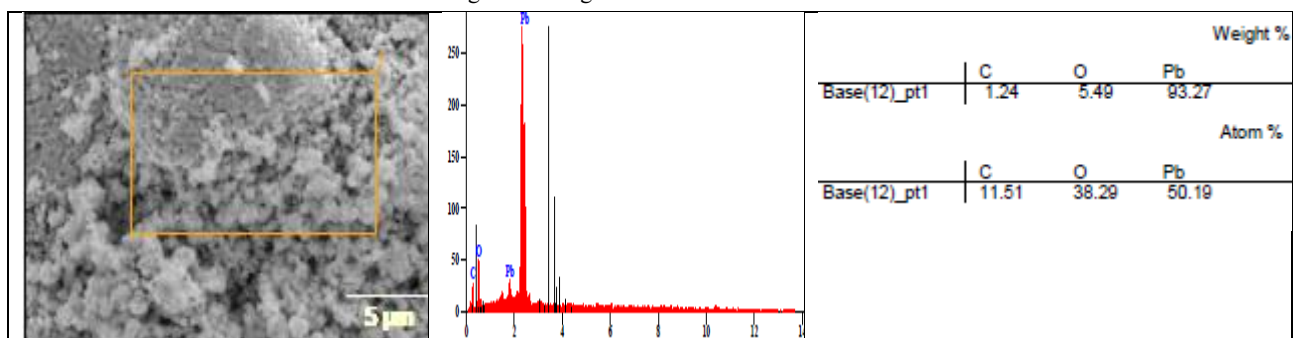


Table 9. SEM image of the negative active mass after calcination at 600°C.



As can be seen in **Table 3**, the raw negative battery paste exhibited irregular micron-sized particles with severe aggregation and surface cracking, consistent with its low BET surface area (4 m²/g) and mixed sulfate/oxide composition detected by EDS. Following ammonium carbonate treatment, a remarkable particle size reduction was observed from **Table 4**, accompanied by improved uniformity. This transformation aligns with the disappearance of sulfate by EDS

The transition to well-defined polyhedral particles with smooth surfaces in the final calcined product at 400,450,500,550 and 600°C confirms complete crystallization into phase-pure PbO, as evidenced by sharp FTIR peaks at 482 cm⁻¹ and thermal stability up to 700°C in TGA.

The image analysis of SEM micrographs using ImageJ software (**Figure 3**) provided an average particle size of 1395.15 nm with a standard deviation of 601.85 nm, it can be said that lead oxide has a compact structure forming grains of this size.

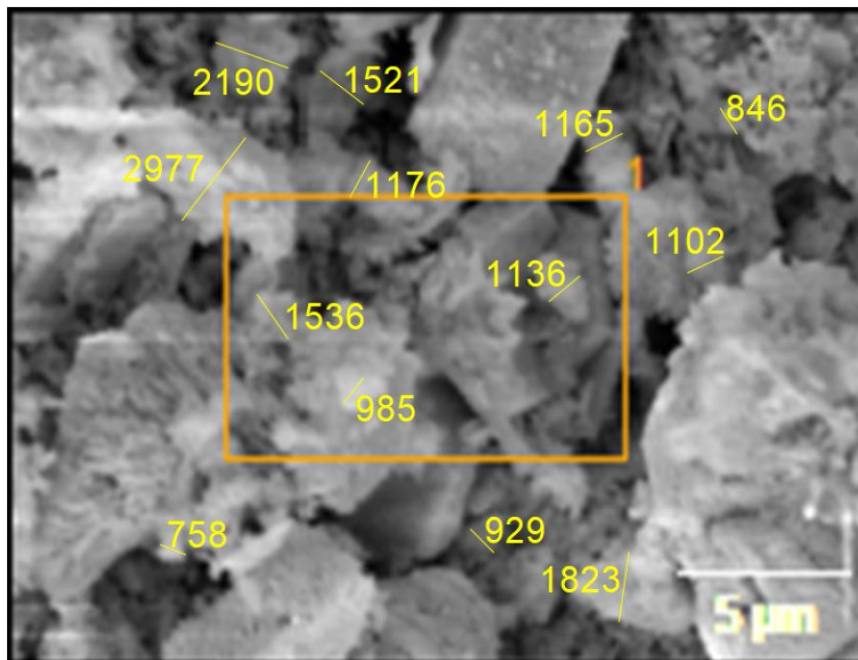


Figure 3. SEM micrograph of the sample calcinated at 450°C.

The progressive morphological refinement - from aggregated micron particles to nanostructured assemblies and finally to discrete nanocrystals - mirrors the chemical purification pathway (sulfate → carbonate → oxide) identified through spectroscopic and thermal analyses. The calcination-induced particle coalescence in 450,500,550 and 600°C, while reducing surface area, produces mechanically robust crystallites suitable for electrode applications.

This multiscale SEM characterization provides crucial structure-processing-property relationships, demonstrating how controlled chemical and thermal treatments can transform battery waste into functional nanomaterials with tailored architectures. The observed morphological features directly account for the measured surface areas, pore characteristics, and thermal behaviors, offering a comprehensive framework for optimizing PbO nanostructure synthesis.

3.6. EDS analysis

The EDS results provide essential elemental composition data that complement our previous FTIR, DRX, and TGA findings, offering a comprehensive understanding of the chemical evolution during PbO synthesis from spent lead-acid battery paste. The analysis reveals systematic changes in lead, oxygen, carbon, and impurity content across the synthesis stages, directly correlating with the structural and thermal transformations observed earlier. **Table 1** summarizes the quantitative data obtained from EDS analysis.

Table 10. EDS elemental composition evolution.

Sample	Pb (wt.%)	O (wt.%)	C (wt.%)	S (wt.%)
Negative active masse	74.07	15.63	--	10.31

After desulfation	83.7	13.06	3.25	–
Calcination at 400°C	89.68	8.92	1.4	–
Calcination at 450°C	92.42	6.47	1.11	–
Calcination at 500°C	94.08	4.83	1.03	--
Calcination at 550°C	93.32	5.95	1.09	--
Calcination at 600°C	93.27	5.49	1.24	--

Table 10. (Continued)

Following desulfation, the EDS data indicate a notable reduction in sulfur content (below detection limits), confirming successful sulfate removal—a finding consistent with the disappearance of sulfate FTIR bands (1122, 619 cm^{-1}) and the appearance of carbonate peaks (820 cm^{-1}).

The calcined sample at 450, 500, 550, and 600°C exhibits a lead-rich composition (~ 94 wt.%, with reduced carbon (~ 1 wt.%), confirming the combustion of organic residues during high-temperature treatment—consistent with TGA’s final mass loss. The oxygen content (~ 6 wt.%) stabilizes, reflecting the formation of stoichiometric PbO, as supported by FTIR’s well-defined Pb–O vibration (482 cm^{-1}). The residual carbon suggests minor surface adsorbates.

3.7. BET analysis

The surface area and porosity characteristics of nanostructured materials significantly influence their chemical reactivity, catalytic efficiency, and adsorption capabilities. The Brunauer-Emmett-Teller (BET) method is widely employed to determine the specific surface area of porous materials by analyzing nitrogen adsorption-desorption isotherms at cryogenic temperatures (-196.345 °C)^[28].

Additionally, the Barrett-Joyner-Halenda (BJH) method is used to assess the pore size distribution, which is crucial in defining the material's adsorption behavior and diffusion properties^[27]. This study focuses on the BET surface area and porosity analysis of nanostructured PbO obtained from recycled lead-acid battery negative plates. **Figure 4** represents the nitrogen adsorption-desorption behavior of the sample. The nitrogen adsorption-desorption isotherm classifies the material's pore structure according to the IUPAC standards^[32]. Figure 4 exhibits the shape of a Type IV isotherm with H3 hysteresis, typical of mesoporous materials^[29]

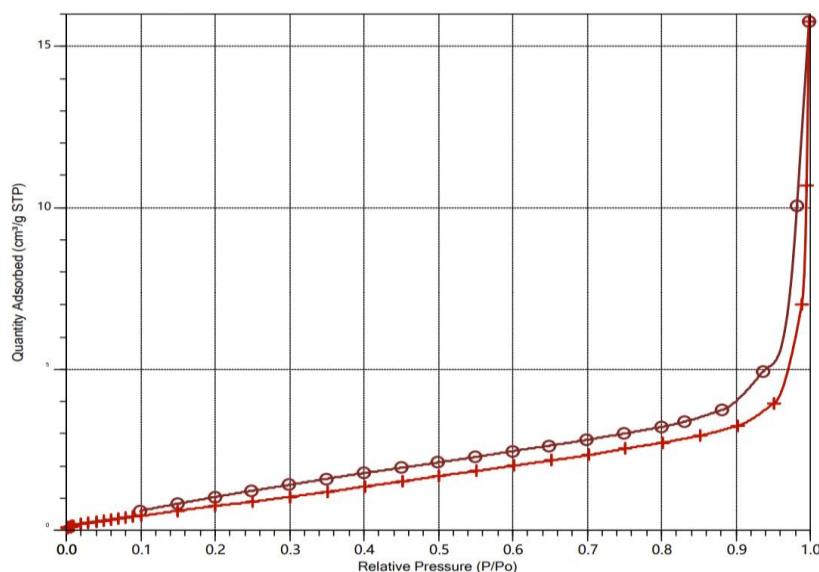


Figure 4. Nitrogen adsorption-desorption isotherms of the sample.

The quantitative results of the performed BET and BJH analysis for the nanostructured PbO are reported in **Table 11**.

Table 11. Quantitative results of BET and BJH analysis for nanostructured PbO.

Parameter	Value	Unit
BET Surface Area	4.0066	m ² /g
Single-Point Surface Area (P/Po = 0.25)	2.8943	m ² /g
Langmuir Surface Area	31.77	m ² /g
t-Plot External Surface Area	6.6719	m ² /g
Total Pore Volume (Adsorption, P/Po = 0.95)	0.006057	cm ³ /g
Total Pore Volume (Desorption, P/Po = 0.95)	0.007977	cm ³ /g
BJH Adsorption Average Pore Diameter	14.1761	nm
BJH Desorption Average Pore Diameter	10.6115	nm

In **Table 11**, the specific surface area, using equation (7):

$$S = n_m N_A A / m \quad (7)$$

where S is the surface area (m²/g), n_m is the monolayer capacity (mol), N_A is Avogadro's number (6.022 × 10²³ mol⁻¹), A is the molecular cross-sectional area of N₂ (0.162 nm²) and m is the sample mass (g). Therefore, the BET surface area is derived from the linear region of the BET plot, which correlates monolayer adsorption coverage with relative pressure [28]. Accordingly, the BET surface area was equal to about 4 m²/g that is a relatively significant value. The significant difference between the Langmuir and BET values suggests that the PbO sample possesses a heterogeneous surface with multilayer adsorption phenomena. The pore size distribution was analyzed using the BJH method, revealing a predominance of mesopores (2-50 nm) [27]. The slightly higher adsorption pore volume compared to desorption is indicative of ink-bottle pore structures [30]

The average particle size (Δ) is estimated using the BET equation (8):

$$\Delta = 6000 / \rho S \quad (8)$$

where ρ is the material density (g/cm³), assumed to be 1.000 g/cm³ and S is the BET surface area (m²/g). Accordingly, the average particle size for the sample is about 1497 nm, which falls within the range reported for PbO nanoparticles [33]. Comparative analysis with previously reported PbO nanostructures indicates that BET surface areas range from 3 to 15 m²/g depending on synthesis conditions and precursor sources. The values obtained in this study align with thermally treated PbO from battery recycling processes [31]

4. Discussion

In this study, the particle size of PbO was evaluated using the BET method, scanning electron microscopy (SEM), and X-ray diffraction (XRD). The BET analysis estimated the particle size to be 1497 nm, while image analysis of SEM micrographs using ImageJ software (**Figure 3**) provided an average particle size of 1395.15 nm with a standard deviation of 601.85 nm. These values indicate good agreement between the two techniques, reinforcing the reliability of the measured particle size. However, a significant difference is observed when compared to the crystallite size obtained from XRD analysis, which yielded a value of 26.38 nm.

The discrepancy between the BET/SEM particle size and the XRD crystallite size arises from the fundamental differences in what these techniques measure. XRD provides information on the crystallite size, which represents the size of a single coherent diffracting domain or the smallest structural unit within the material. In contrast, SEM and BET methods measure the aggregate or particle size, which often consists of multiple crystallites forming larger agglomerates. The high-temperature calcination process at 450°C promotes the growth and aggregation of PbO crystallites, leading to larger secondary particle sizes observed in BET and SEM analyses [31].

Additionally, PbO nanoparticles tend to exhibit strong inter-particle interactions due to their surface energy and electrostatic forces, which further promote agglomeration. This behavior is particularly common in oxide materials, where van der Waals forces and sintering effects contribute to particle growth beyond the nanoscale crystallite dimensions [33,34]. The difference between crystallite size and particle size is a well-documented phenomenon in nanomaterials and highlights the importance of using multiple characterization techniques for a comprehensive understanding of material morphology [35,32]

5. Conclusion

In This research PbSO₄ of the used battery can be fully desulfated by using (NH₄)₂CO₃ to produce PbCO₃, which is then calcined to produce lead oxide. The results show the importance of the temperature of calcination on the nature of products, the 450°C is the best temperature to obtain α-PbO fine powders with particle size of about 26 nm with a mesoporous materials and BET surface area was equal to about 4 m²/g, after this temperature we obtain a mixture of lead oxides.

Conflict of interest

The authors declare no conflict of interest.

References

1. Pan JQ, Sun YZ, Li W et al. A green lead hydrometallurgical process based on a hydrogen-lead oxide fuel cell. *Nat Commun* 4 (2013) 2178
2. Shu YH, Ma C, Zhu LG et al. Leaching of lead slag component by sodium chloride and diluted nitric acid and synthesis of ultrafine lead oxide powders. *J Power Sources* 281 (2015) 219–226
3. Gao PR, Liu Y, Bu XF et al. Solvothermal synthesis of α-PbO from lead dioxide and its electrochemical performance as a positive electrode material. *J Power Sources* 242(2013)299–304
4. Bourgoin Xavier, "Elaboration et caractérisation physico-chimique de nano-composites plomb/céramique pour batteries Acide", Thèse de Doctorat, 2007, Université Henri Poincaré Nancy 1.
5. R. Yousefi, F. Jamali-sheini et al, Facile synthesis and optical properties of PbO, *Latin American Applied Research*, 159-162 (2014)
6. Pan JQ, Sun YZ, Li W et al (2013) A green lead hydrometallurgical process based on a hydrogen-lead oxide fuel cell. *Nat Commun* 4:2178
7. Shu YH, Ma C, Zhu LG et al (2015) Leaching of lead slag component by sodium chloride and diluted nitric acid and synthesis of ultrafine lead oxide powders. *J Power Sources* 281:219–226
8. Gao PR, Liu Y, Bu XF et al (2013) Solvothermal synthesis of α-PbO from lead dioxide and its electrochemical performance as a positive electrode material. *J Power Sources* 242:299–304
9. Behnoudnia, F. and H. Dehghani, "Synthesis and characterization of novel three-dimensional-cauliflowerlike nanostructure of lead (II) oxalate and its thermal decomposition for preparation of PbO," *Inorg. Chem. Commun.*, 24, 32-39 (2012).
10. Singh, D.P. and O.N. Srivastava, "Synthesis of micron-sized hexagonal and flowerlike nanostructures of lead oxide (PbO₂) by anodic oxidation of lead," *Nano and Micro Letters*, 3, 223-227 (2011).
11. Soltanian Fard, M.J., F. Rastaghi and N. Ghanbari, "Sonochemical synthesis of new nano-two-dimensional lead (II) coordination polymer: As precursor for preparation of PbO nano-structure," *J. Mol. Struct.*, 1032, 133-137 (2013).
12. Jia, B. and L. Gao, "Synthesis and characterization of single crystalline PbO nanorods via a facile hydrothermal method," *Mater. Chem. Phys.*, 100, 351-354 (2006).
13. Li, L., X. Zhu, D. Yang, et al, "Preparation and characterization of nano-structured lead oxide from spent lead acid battery paste," *J. Hazard. Mater.*, 203-204, 274-282 (2012)
14. Awwad, A. M.; Albiss, B. Biosynthesis of Colloidal Copper Hydroxide Nanowires Using Pistachio Leaf Extract. *AML*. 2015, 6, 51–54. DOI: 10.5185/amlett.2015.5630.
15. Thankalekshmi, R. R.; Dixit, S.; Rastogi, A. C. Doping Sensitive
16. Optical Scattering in Zinc Oxide Nanostructured Films for Solar Cells. *Adv. Mater. Lett.* 2013, 4, 9–14. DOI: 10.5185/amlett.2013.icnano.137.
17. M. Thommes, K. Kaneko, A. V. Neimark, J.P. Olivier, F. Rodriguez-Reinoso, J. Rouquerol, K.S.W. Sing, Physisorption of gases, with special reference to the evaluation of surface area and pore size distribution (IUPAC Technical Report), *Pure Appl. Chem.* 87 (2015) 1051–1069. <https://doi.org/10.1515/pac-2014-1117>
18. Wang YG, Lin XH, Zhang H et al Selected-control hydrothermal growths of α- and β-PbO crystals and orientated pressure induced phase transition. *CrystengComm* (2013) 15:3513–3516

19. Wei Liu¹, Beibei Ma... et al, Electrochemical property of α -PbO prepared from the spent negative powders of lead acid batteries, Springer-Verlag Berlin Heidelberg 2016
20. L.T. Lam, I.G. Mawston, D. Pavlov, D.A.J. Rand, J. Power Sources 48 (1994) 257e268
21. J. Wang, S. Zhong, H.K. Liu, S.X. Dou, J. Power Sources 113 (2003) 371e375.
22. Zhu XF, Li L, Sun XJ et al (2012) Preparation of basic lead oxide from spent lead acid battery paste via chemical conversion. Hydrometallurgy 117:24–31
23. [21] S.A.A. Sajadi, A.A. Alamolhoda, Inorg. Mater. 42 (2006) 1099e1103.
24. I.A.D. Al-Hydary, A.M. Abdullah, M.A.A. Al-dujaili, Utilizing the cold sintering process for sintering the thermally decomposable lead dioxide, J. Aust. Ceram. Soc. 56 (2020) 139–148. doi:10.1007/s41779-019-00432-5.
25. K.C. Sk. Khadeer Pasha, L. John Kennedy, J. Judith Vijaya, Humidity Sensing Behaviour of Nanocrystalline α -PbO Synthesized by Alcohol Thermal Process, Sensors Transducers J. 122 (2010) 20–27.
26. V. Timar, R. L. Ciceo, I. Ardelean, Structural studies of iron doped $3\text{B}_2\text{O}_3 \cdot 0.7\text{PbO} \cdot 0.3\text{Ag}_2\text{O}$ glasses by FT-IR and Raman spectroscopies., Semicond. Physics, Quant. Elect. Optoelect. 11 (2008) 221.
27. Barrett, E. P., Joyner, L. G., & Halenda, P. P. (1951). The determination of pore volume and area distributions in porous substances. Journal of the American Chemical Society, 73(1), 373-380.
28. Brunauer, S., Emmett, P. H., & Teller, E. (1938). Adsorption of gases in multimolecular layers. Journal of the American Chemical Society, 60(2), 309-319.
29. Yadav et al. (2019). Maleic Anhydride Cross-Linked β -Cyclodextrin-Conjugated Magnetic Nano-adsorbent: An Ecofriendly Approach for Simultaneous Adsorption of Hydrophilic and Hydrophobic Dyes, ACS Omega.
30. Lowell, S., Shields, J. E., Thomas, M. A., & Thommes, M. (2004). Characterization of Porous Solids and Powders: Surface Area, Pore Size, and Density. Springer.
31. Ryu, Z., Zhang, L., & Chen, X. (2017). Structural and morphological evolution of PbO from recycled lead-acid battery materials. Materials Chemistry and Physics, 203, 256-262.
32. Sing, K. S. W., Everett, D. H., Haul, R. A. W., Moscou, L., Pierotti, R. A., Rouquerol, J., & Siemieniewska, T. (1985). Reporting physisorption data for gas/solid systems. Pure and Applied Chemistry, 57(4), 603-619.
33. Zhang, T., Wang, Y., Li, H., & Liu, X. (2020). Influence of synthesis methods on PbO nanostructures for energy applications. Nano Research, 13(5), 1024-1034.
34. Gregg, S. J., & Sing, K. S. W. (1982). Adsorption, Surface Area, and Porosity. Academic Press.
35. Patterson, A. L. (1939). The Scherrer formula for X-ray particle size determination. Physical Review, 56(10), 978.
36. Javidparvar AA, Naderi R, Ramezanzade B. Incorporation of Graphene Oxide Nanoparticles Modified with Benzimidazole into an Epoxy Polyamide Coating to Enhance the Physical-Mechanical Properties. Journal of Color Science and Technology 2020;13:341–52. <https://doi.org/10.1039/C6CP01531J>
37. Zhang Y, Feng C, Zhang Y, Wu H, Liu T. Synthesis and electrochemical performance of $\text{Pb}_3(\text{OH})_2(\text{CO}_3)_2/\text{C}$ anode material for lithium-ion battery application. Ionics (Kiel) 2020;26:3289–95. <https://doi.org/10.1007/s11581-019-03417-3>.
38. Chen Y, Kong Z, Chen W, Xiao L, Yuan Y, Li Z, et al. In situ synthesis of high dielectric constant GNPs/PBO nanocomposites with enhanced thermostability. IET Nanodielectrics 2019;2:97–102.